Available online at www.sciencedirect.com
ScienceDirect
Trans. Nonferrous Met. Soc. China 34(2024) 1191−1203
Transactions of Nonferrous Metals Society of China
www.tnmsc.cn

Effects of shell mold heating temperature on microstructures and freckle formation of single crystal superalloys

Zhi-cheng WANG, Jia-rong LI, Shi-zhong LIU, Wan-peng YANG, Xiao-guang WANG

Science and Technology on Advanced High Temperature Structural Materials Laboratory,
Beijing Institute of Aeronautical Materials, Beijing 100095, China

Received 24 October 2022; accepted 15 May 2023

Abstract: To study the effects of shell mold heating temperature on the microstructure and freckle formation of single crystal superalloys, the directional solidification experiment and simulation were conducted with designed stepwise specimens. The temperature field and morphology of mushy zone were analyzed. The results show that the primary and secondary dendrite arm spacings both decrease with the rise of shell mold heating temperature. This reduces the permeability of the liquid in the mushy zone and the width of the thermal-solutal convection channel, which reduces the formation tendency of freckles, the width of freckles and the number of dendritic fragments in freckled areas. In addition, with the increase of shell mold heating temperature, the cooling rate of liquid in the mushy zone increases, which reduces the cooling time of the melt in the mushy zone, weakens the breaking capability of liquid flow to the dendrite, and further reduces the tendency of freckle formation in single crystal superalloy castings.
Key words: single crystal superalloy; freckle formation; shell mold heating temperature; directional solidification; numerical simulation

1 Introduction

Due to their excellent comprehensive mechanical properties at elevated temperature, nickel based single crystal superalloys are widely used in the preparation of turbine blades for aero-engines [1−4]. With the development of aero-engines, higher and higher demands are placed on single crystal superalloys. This has led to an increase in the content of refractory alloying elements in single crystal superalloys, together with the increasing complexity of the turbine blade structure. These have promoted the formation of grain defects in the manufacture process of turbine blades [5].

The main grain defects occurring in directional solidification of turbine blades include stray grains [6], freckles [7], sliver defects [8] and low angle grain boundaries [9]. Freckles tend to appear in the directional solidification process of single crystal superalloy specimens especially for the specimens with a complex structure. Due to the nature of macroscopic segregation, once freckles are formed on the casting they cannot be removed by subsequent thermo-mechanical treatment, which will adversely affect the performance of the castings [10]. Therefore, it is of great importance to study the factors that influence freckle formation, which helps to further understand the mechanism of freckle formation and to develop effective control methods.

It is widely believed that freckles are caused by thermal-solutal convection in the mushy zone originating from alloying elements segregation [11−13]. Freckles usually present as long chains on the surface of the specimens, consisting of the disorderly oriented dendritic

Corresponding author: Jia-rong LI, Tel: +86-10-62497202, +86-10-62498314, E-mail: jrli126@126.com
DOI: 10.1016/S1003-6326(24)66463-0

fragments and eutectics [14]. So far, numerous researches have been concentrated on the factors that affect the freckle formation of single crystal superalloys, such as chemical composition [15,16], geometry of the specimens [17,18], solidification process parameters [19,20], and crystal orientation [21]. In the preparation of turbine blades, the metal liquid is poured into the pre-heated shell mold and then slowly withdrawn towards the cooling zone at a set withdrawal velocity. Researches show that the heating temperature of the shell mold has a significant influence on temperature gradient and solidification rates of the casting [22]. The curvature of the isotherm varies with process parameters and affects the local thermal conditions, thereby affecting the morphological evolution of dendritic structures during solidification [23].

However, researches on the effects of process parameters on freckle formation have been mainly focused on the withdrawal rate, and less work has been conducted on the effects of heating temperature of the shell mold on freckle formation, which is an important and easily adjustable parameter during the directional solidification. Therefore, in this work, the effects of heating temperature of the shell mold on the formation of freckles were investigated by a newly designed stepwise specimen to further understand the formation mechanism of freckles in single crystal superalloys. In addition, a commercially available finite element model ProCast^{TM} was employed to simulate the directional solidification process so as to provide insight into the effects of shell mold heating temperature on freckle formation. This study will provide theoretical guidance for the control of freckles in the manufacture process of turbine blades.

2 Experimental

2.1 Materials and specimen preparation

The third generation single crystal superalloy, DD9, was used in this research. The compositions of DD9 alloy are given in Table 1 [4]. The stepwise specimen designed to study the effects of casting size on the formation of freckles was used here. Its geometry and size are shown in Fig. 1(a). The stairs along the solidification direction are named as the first stair, the second stair, and the third stair. The heights of the first, second and third stairs are 30, 30 and 50 mm while the side lengths are 26, 18 and 10 mm, respectively. Three stairs with different sizes represent different sizes of parts on the turbine blades.

Table 1 Compositions of single crystal superalloy DD9 (wt.%) [4]

Cr	Co	Mo	W	Re	Al
3.5	7	2	6.5	4.5	5.6
Ta	Nb	Hf	C	Y	Ni
7.5	0.5	0.1	0.008	0.001	Bal.

Bridgman method was used to manufacture the stepwise specimens. The directional solidification processing was carried out by high rate solidification (HRS) technique. Six wax patterns of specimen were assembled with the sprue cup and runner to form a mold cluster in a *d*200 mm chassis,

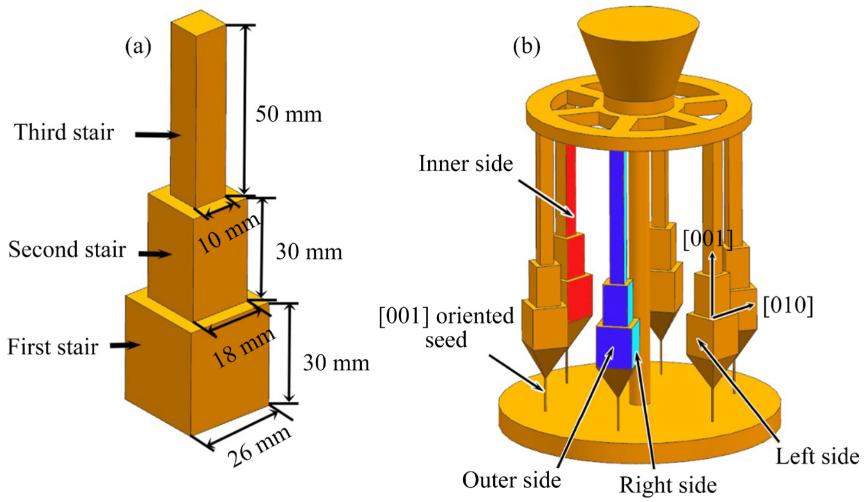

Fig. 1 Geometry and size of stepwise specimen (a) and combination of wax mold (b)

as shown in Fig. 1(b). In order to exclude the influence of crystal orientation on the formation of freckles in single crystal superalloy castings, [001] oriented crystal seeds were employed to obtain single crystal specimens and the secondary orientation [010] was controlled along the edges of the specimen, as shown in Fig. 1(b). For the convenience of the following description, the inner side, the outer side, the left and right side were defined, as shown in Fig. 1(b). The inner side of the specimens refer to the side facing the center of the mold cluster, and the outer side refers to the side facing the heating area of the directional solidification furnace.

The clusters were first dipped into refractory material slurry and coated with alumina sands and this process was repeated until the thickness of the ceramic shell mold reached 6 mm. The shell mold was dewaxed in a steam dewaxing kettle at 180 °C and 0.9 MPa for 10 min. Then, the shell mold was baked to increase its strength at 900 °C for 2 h, and the residual wax was eliminated at the same time. The master alloy was refined at 1570 °C and maintained at this temperature for 5 min before being poured into the shell molds. The shell molds were heated to two different temperatures of 1510 and 1570 °C before pouring to study the effects of heating temperature of shell mold on freckle formation. The pouring temperature under two conditions is the same as the heating temperature of the shell molds. At last, the mold was withdrawn downward at 2 mm/min from the heat zone to the cooling zone.

2.2 Microstructure examination

After directional solidification, the specimens were separated from the cluster first and the shell mold on the surface of the specimens was completely cleared. Then, sand blasting and macro-etching were performed to reveal the morphology of freckles. A ruler with a scale of 0.5 mm was used to measure the length of freckles. After macroscopic corrosion of the specimens, the number of freckle chains was counted. The clearly visible independent chains, including the freckle chains that appeared at the edges of the specimens were all needed to be counted. OM and FEI Nova450 FE-SEM were used to analyze the microstructure of the freckled area. Metallographic analysis software Image-pro Plus 6.0 was used to measure the primary dendrite arm spacing, the width of the freckle chains and the volume fraction of eutectics. The primary dendrite arm spacing (PDAS, λ_1) was calculated using the equation $\lambda_1=(S/N)^{0.5}$, where S is the area of the selected field of view and N is the number of primary dendrites arm in the field of view. The result of primary dendrite arm spacing and the volume fraction of eutectics was obtained from the average value of at least 5 measurements. Samples for microstructural observation were firstly polished and then etched with 80 mL HCl + 25 g $CuSO_4$ + 100 mL H_2O for 4−8 s.

2.3 Numerical simulation

Finite element simulation software Pro-CAST was used to analyze the thermal field and morphology of the mushy zone at different shell mold heating temperatures to better understand the influence of shell mold heating temperature on freckle formation. The morphologies of the mushy zone were visualized with the post-processing module. Three-dimensional model used in the simulation is shown in Fig. 2. In view of symmetry, only 1/6 of the model was considered here to improve computational efficiency. Radiation baffle, chill plate, water-cooled rings, shell mold, heating zone and cooling zone were constructed here. The cooling curves of the specimen were obtained by means of thermocouples pre-positioned in the shell mold and the two temperature measuring points were set in the center of the outer side of the first stair in two different specimens.

Boundary conditions and initial conditions for simulation are listed in Table 2, which were originated from our previous research [24]. The

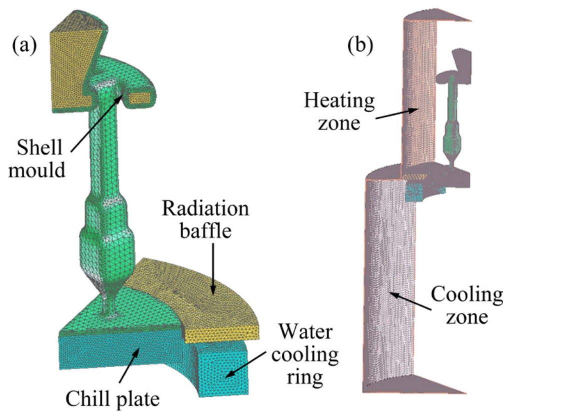

Fig. 2 Three-dimensional model for simulation: (a) 1/6 three-dimensional model; (b) Finite element surface mesh for heating and cooling zones

Table 2 Boundary conditions and initial conditions for simulation in two different processing conditions [24]

Parameter	Value
Temperature of heating zone/°C	1510, 1570
Emissivity of heating zone	0.90
Temperature of cooling zone/°C	25
Emissivity of cooling zone	0.4
Temperature of chill-plate/°C	25
Emissivity of chill-plate	0.4
Temperature of shell mold/°C	1510, 1570

heat transfer coefficients were set between the shell mold and specimen, specimen and chill plate, shell mold and chill plate. The value of interface heat transfer coefficient (IHTC) was assumed to change with temperature. The density, thermal conductivity and other thermophysical properties for superalloy DD9 came from literature [25].

3 Results

3.1 Freckle formation at different shell mold heating temperatures

The formation of freckles at different shell mold heating temperatures is shown in Fig. 3 and the statistical results are listed in Table 3 and Fig. 4. It can be observed that freckle chains are formed on the outer side of the first stair including the two outer edges at the shell mold heating temperature of 1510 °C (Fig. 3(a)). Most of the freckle chains are slanted towards the nearby edges. Not any freckle chain is formed on the left, right and inner sides of the specimen, but short freckle chains are formed in the two inner side edges of the specimen, as marked with dashed oval circle in Fig. 3(a_4). It should be pointed out that the average length of freckle chains on the two edges of the inner side is 8 mm which is significantly shorter than 23 mm on the two edges of the outer side. When the heating temperature of shell mold rises to 1570 °C, the number of freckle chains appearing on the outer side decreases to 19, and not any freckle is formed on the right, left and inner sides of the specimen either (seen from Fig. 3(b)). It is worth noting that when the heater temperature is 1510 °C, the formation of freckles can cause the formation of a large number of sliver defects, as marked with red arrows in Fig. 3(a_1). When the heater temperature increases to 1570 °C, no any sliver defect is caused by freckles.

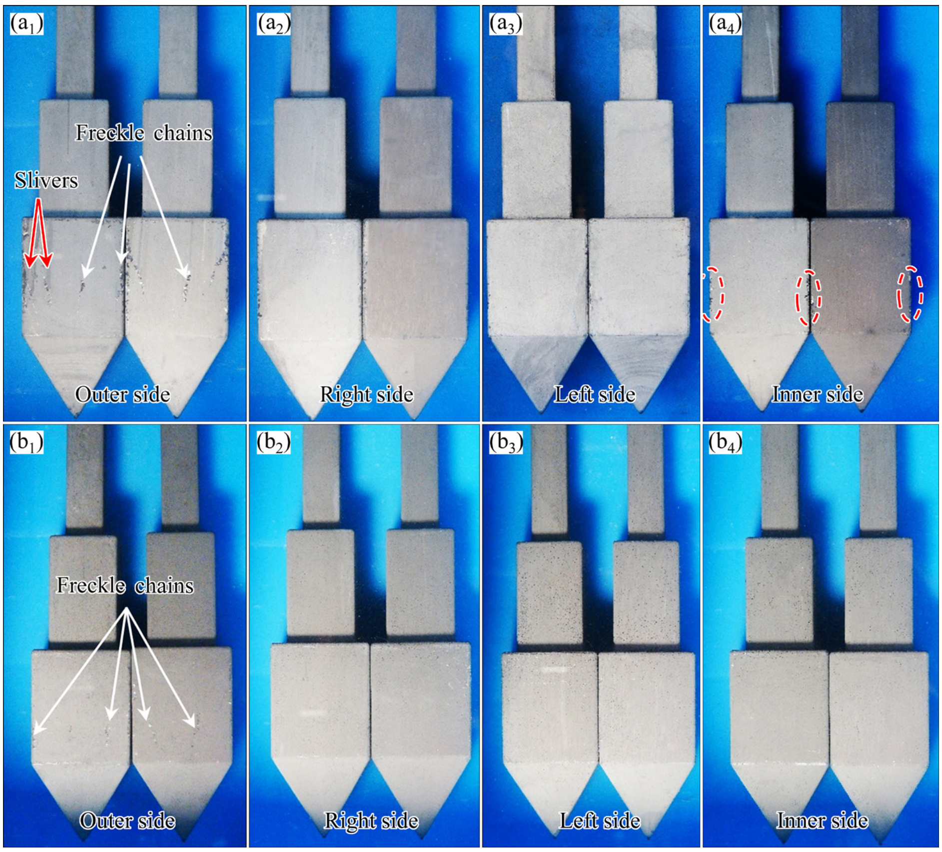

Fig. 3 Formation of freckles in specimens at different shell mold heating temperatures: (a_1–a_4) 1510 °C; (b_1–b_4) 1570 °C

Table 3 Number of freckle chains in specimens at different shell mold heating temperatures

Heating temperature/°C	Number of freckle chains (including edges)		
	Outer side	Inner side	Left/right side
1510	25	12	0
1570	19	0	0

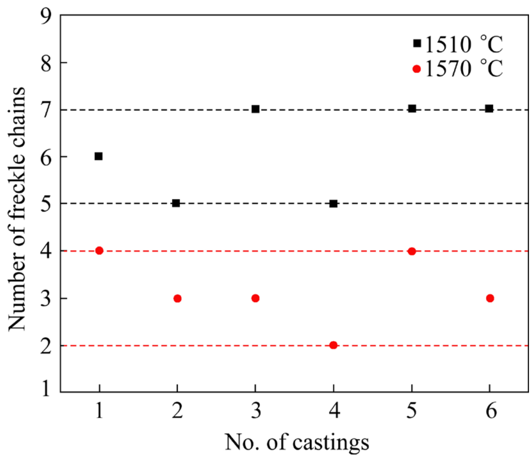

Fig. 4 Number of freckle chains in each specimen

3.2 Microstructure of freckles at different shell mold heating temperatures

The microstructures of freckles at different shell mold heating temperatures are shown in Fig. 5. Figures 5(a, b) show the OM image and SEM image of freckles at the heating temperature of 1510 °C. A large number of dendritic fragments and amounts of eutectics can be observed in freckled area. It is evident that some larger dendritic fragments, as marked by arrows in Fig. 5(a), are originated from the primary dendritic trunk. Figures 5(c, d) show the OM image and SEM image of freckles at the heating temperature of 1570 °C. Similarly, a certain number of dendritic fragments and a great deal of eutectics appear in freckled zone. However, the number of dendrite fragments is significantly less than that at the heating temperature of 1510 °C. Figure 6 shows the distribution of the measured freckle chain width at different shell mold heating temperatures. The freckle chains have an average width of 799 μm at the heating temperature of 1510 °C which is larger than that of 476 μm at the heating temperature of 1570 °C. The secondary dendritic arm spacing (SDAS, λ_2) is measured to be 83 μm at the heating temperature of 1510 °C and 71 μm at the heating temperature of 1570 °C.

Figure 7 shows the transverse microstructure at 8 mm above the bottom edge of the first stair at

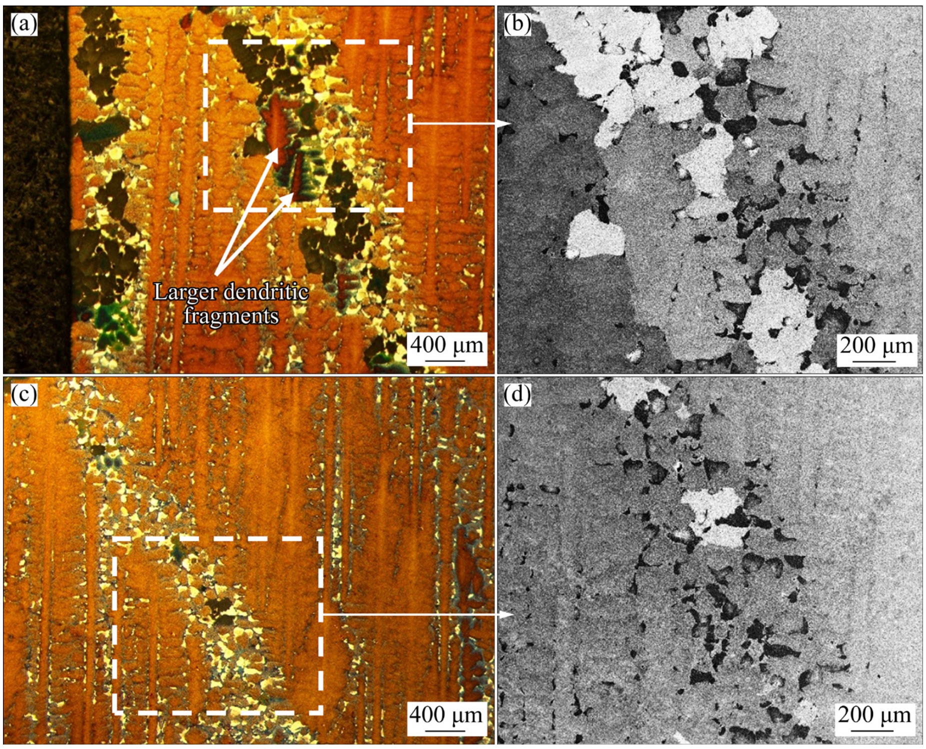

Fig. 5 Longitudinal microstructures of freckle chains at different shell mold heating temperatures: (a) OM image of freckles at 1510 °C; (b) SEM image of freckles at 1510 °C; (c) OM image of freckles at 1570 °C; (d) SEM image of freckles at 1570 °C

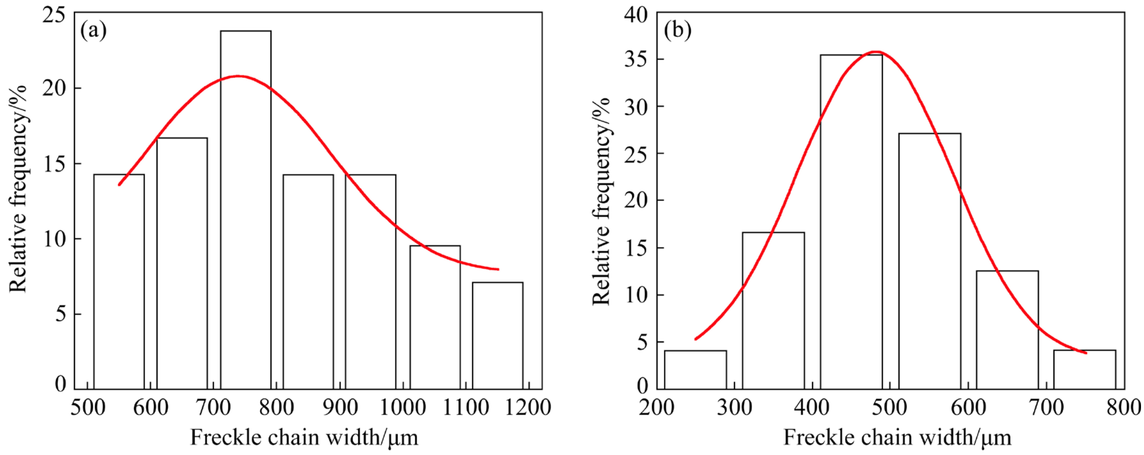

Fig. 6 Distribution of freckle chain width at different shell mold heating temperatures: (a) 1510 °C; (b) 1570 °C

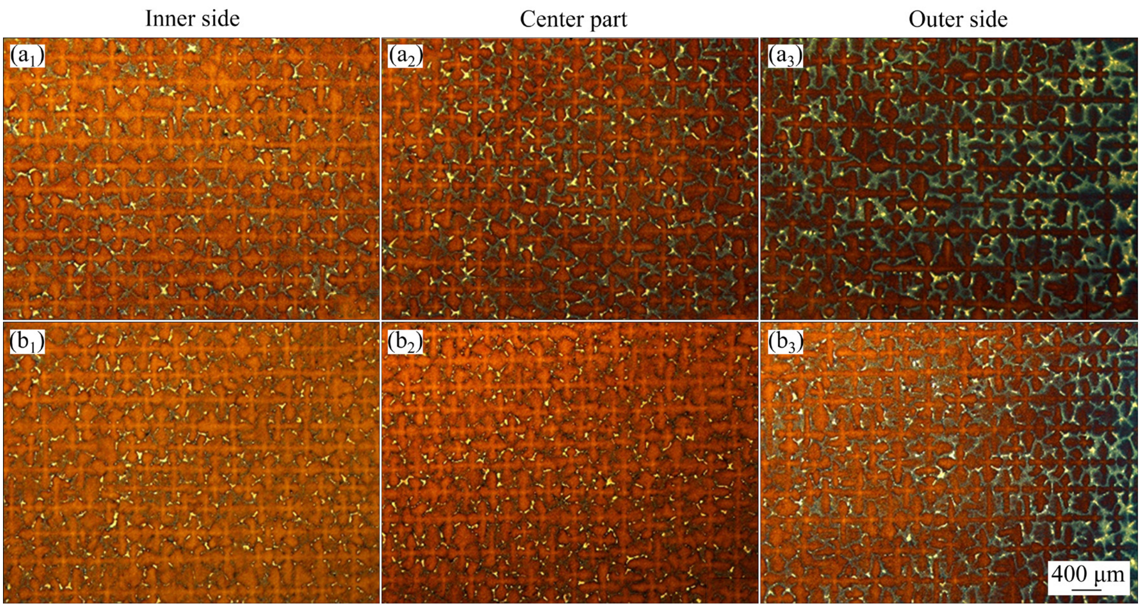

Fig. 7 Dendrite structure in different parts of cross section at 8 mm above first stair at different heating temperatures: (a_1–a_3) 1510 °C; (b_1–b_3) 1570 °C

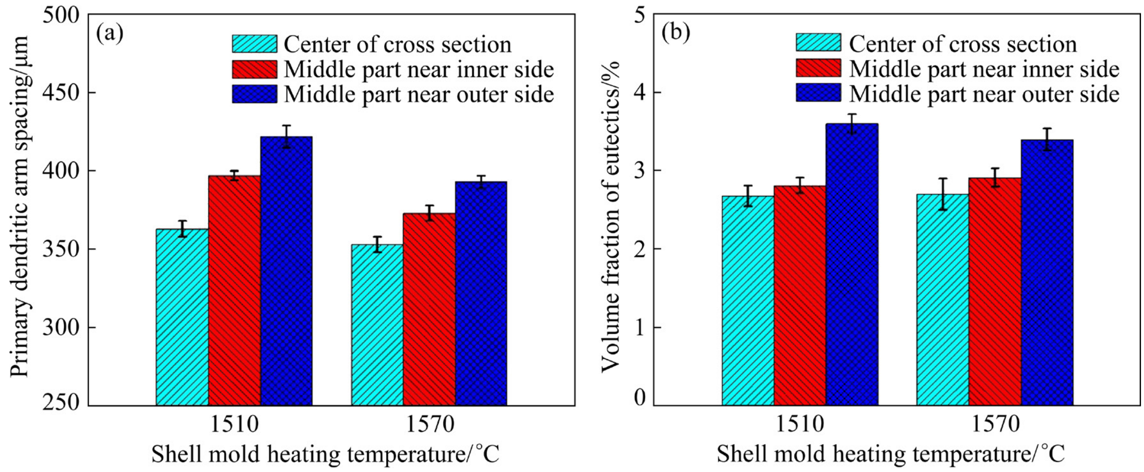

Fig. 8 Primary dendritic arm spacing (a) and volume fraction of γ–γ' eutectics (b) in different parts on cross section at 8 mm above first stair at different heating temperatures

different heating temperatures. The primary dendritic arm spacing (PDAS) and the content of eutectics are shown in Fig. 8. It is suggested that the PDAS near the outer side is much larger than that near the inner side and the PDAS near the inner side is much larger than that in the center part of the cross section. The situation is the same at two different heating temperature conditions. By comparing the PDAS at two different heating temperatures, it can be observed that the difference of PDAS in the center region is very small. The discrepancy of the PDAS is highlighted in the middle near the outer side and the inner side. The PDAS decreases as the heating temperature increases. It is worth noting that the secondary dendritic arm near the outer side is slimmer than that of the center and near the inner side. The different characteristics showing in dendritic morphology reflect the difference in the thermal condition in the directional solidification.

3.3 Simulation results

The temperature measurement was conducted on two symmetrically distributed specimens in the cluster at the heating temperature of 1510 °C and the two measured points are both located in the midpoint of the outer side of the first stair, as marked with arrow in Fig. 9. The measured and calculated results of the cooling curves are compared in Fig. 9. The maximum discrepancy above 1300 °C between the measured and calculated temperatures is only 22 °C, which accounts for 1.6% of the temperature value. Therefore, the simulation results are considered reliable and can represent the cooling situation of the actual directional solidification process of the specimen.

Due to the symmetry of the temperature field on right and left sides of the specimen, only the morphology of the mushy zone on the right side of the specimen at different heating temperatures are shown here, which can be seen in Fig. 10. Average heights (h) of the mushy zone and inclination angles (θ) of different solidification stages at different heating temperatures are listed in Tables 4 and 5 and shown in Fig. 11 (The inclination angle θ here is defined as the included angle between the connecting line of two endpoints of the isotherm and the horizontal line, as marked in Fig. 10(b)). When the solidification progressed to the first stair at the heating temperature of 1510 °C, the mushy zone was at the lower edge of the baffle and the isotherm inclined from the outer side to the inner side. When the heating temperature increased to 1570 °C, the mushy zone further moved downward relative to the baffle and the isotherm inclined still from the outer side to the inner side. At the same time, the height of the mushy zone was significantly reduced and the tilt angle of the isotherm was only slightly increased.

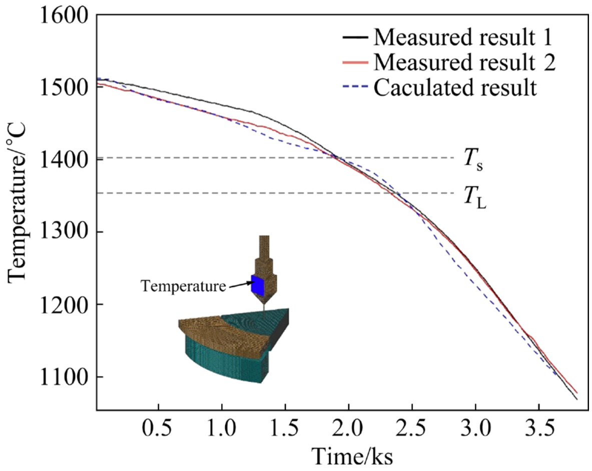

Fig. 9 Comparison of measured and calculated cooling curves

When the second stair solidified, the mushy zone moved upward relative to the baffle at both heating temperatures, and it arrived at the upper edge of the baffle at the heating temperature of 1510 °C, but the mushy zone was still underneath the baffle at the heating temperature of 1570 °C. The heights of the mushy zone and the inclination angles of the isotherm both decreased evidently compared to the first stair. Although the isotherm inclined still from the outer side to the inner side, the curvature of the isotherm was significantly reduced. The heights of the mushy zone were still smaller at 1570 °C compared to 1510 °C, but the difference in the tilt of the isotherms was not significant.

When the third stair solidified, the mushy zone moved up further relative to the baffle, and it reached the upper edge of the radiation baffle under both heating temperature conditions. The width of the mushy zones further decreased and the isotherms became almost horizontal. The rates at which the front of the mushy zone moved forward were (2.1±0.1) mm/min at both shell mold heating temperatures.

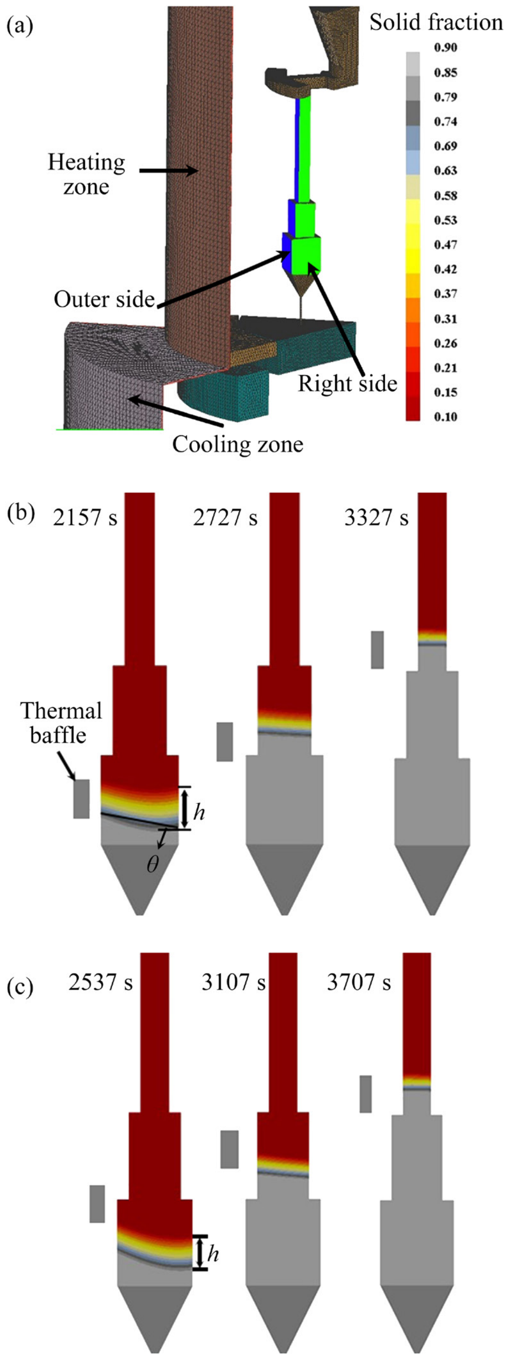

Fig. 10 Morphology of isotherm in mushy zone on right side of specimen: (a) Schematic diagram of cluster; (b)1510 °C; (c) 1570 °C

Table 4 Average height of mushy zone (mm)

Heating temperature/°C	First stair	Second stair	Third stair
1510	14.8±1.0	10.3±0.3	8.5±0.2
1570	11.2±0.8	8.8±0.3	8.2±0.2

Table 5 Average inclination angle of isotherm in mushy zone (°)

Heating temperature/°C	First stair	Second stair	Third stair
1510	7.3±0.5	4.3±0.3	1.2±0.2
1570	7.6±0.6	4.4±0.3	1.3±0.2

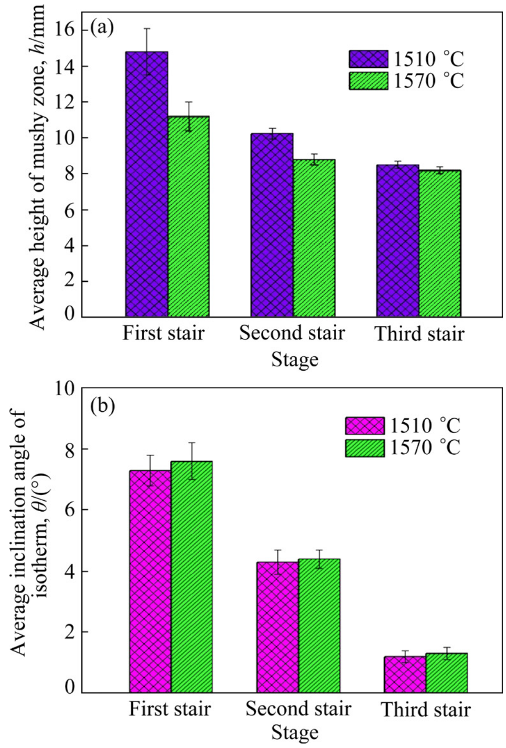

Fig. 11 Characteristic parameters of morphology in mushy zone: (a) Average height (h); (b) Average inclination angle (θ)

The temperature gradient in the liquid ahead of the solid/liquid interface (G_L) at different solidification stages was calculated, and the results are shown in Fig. 12(a) and listed in Table 6. It is suggested that as the heating temperature of the shell mold increases, the temperature gradient (G_L) increases at the same solidifying stages. The cooling rate (V) of the melt in the mushy zone can be calculated by

$$V=G_L R \tag{1}$$

where R is the solidification rate which is approximately the same as the withdrawal rate of 2 mm/min at the two different heating temperatures. The cooling rate (V) of the liquid in the mushy zone at different heating temperatures are shown in Fig. 12(b) and listed in Table 7. The results show that the increase of the heating temperature leads to the accelerated cooling of the liquid in the mushy zone.

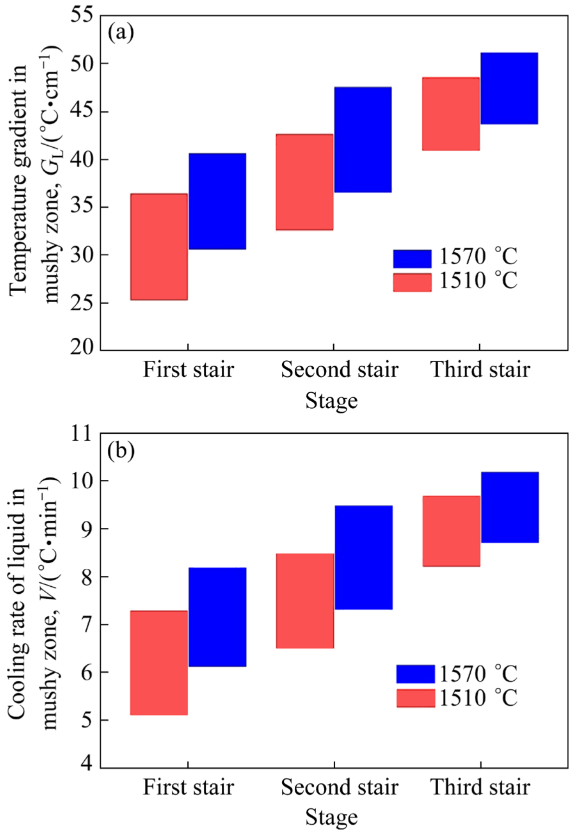

Fig. 12 Temperature gradient (G_L) (a) and cooling rate of liquid (V) (b) in mushy zone at different solidification stages at two heating temperatures

Table 6 Temperature gradient (G_L) in liquid phase at front of solidification interface (°C/cm)

Shell mold heating temperature/°C	First stair	Second stair	Third stair
1510	25.2−36.5	32.5−42.7	40.9−48.6
1570	30.5−40.7	36.5−47.6	43.7−51.2

Table 7 Cooling rate (V) of liquid at front of mushy zone (°C/min)

Shell mold heating temperature/°C	First stair	Second stair	Third stair
1510	5.1−7.3	6.5−8.5	8.2−9.7
1570	6.1−8.2	7.3−9.5	8.7−10.2

4 Discussion

4.1 Analysis of thermal simulation

The Bridgman technology relies on radiation to dissipate heat from the specimen. When the mushy zone is below the thermal baffle in the solidification (Figs. 10(b, c)), the outer side of the specimen facing the cooling zone can be cooled more effectively than the inner side of the specimen facing the center of the mold cluster. Therefore, the isotherm inclines from the outer side to the inner side, which results in a sloping state of the mushy zone as a whole. The further the mushy zone is below the baffle, the greater the difference becomes in cooling efficiency between the inner side and the outer side. As the shell mold heating temperature increases from 1510 to 1570 °C, the thermal baffle moves upward with respect to the mushy zone when the first stair solidifies (Fig. 10), so the average inclination angle (θ) of the mushy zone slightly increases (Fig. 11(b)). When solidification proceeds to the second stair and the third stair, the mushy zone moves upward to the vicinity of the thermal baffle, and the temperature distribution between the outer side and inner side becomes uniform, so the inclination of the isotherm is further reduced (Fig. 11(b)).

The increase of the heating temperature widens the temperature difference between the heating zone and the cooling zone of the directional solidification furnace. This results in an increased temperature gradient in the mushy zone during the directional solidification process (Table 6 and Fig. 12(a)). So, the height of the mushy zone increases as the heating temperature of the shell mold rises (Fig. 11(a)).

Under the same solidification velocity, the melt cooling rate in the mushy zone grows with the increase of the temperature gradient (G_L) (Table 7 and Fig. 12(b)), so the cooling rate of the melt in the mushy zone increases with the rise of the heating temperature. When the solidification progresses to the second and third stair, the size of the specimen is reduced, which leads to a faster cooling of the specimen (Table 7 and Fig. 12(b)), so the mushy zone moves upward relative to the radiation baffle (Figs. 10(b, c)). A further reduction in the difference of cooling efficiency between the inner side and outer side flattens the isotherm.

4.2 Effects of heating temperature on microstructure

The PDAS and SDAS, which are defined by the following equations proposed by KURZ and FISHER [26] and HUNT et al [27], respectively, are determined by the temperature gradient (G_L) and solidification rate (R):

$$\lambda_1 = A G_L^{-1/2} R^{-1/4} \tag{2}$$

$$\lambda_2 = B \left(G_L R\right)^{-1/3} \tag{3}$$

where A and B are constants determined by the physical parameters of alloy. In this experiment, the specimen solidified at the same withdrawal rate, so the solidification rate (R) is almost the same. Therefore, the primary and secondary dendrite arm spacings are determined by the G_L. As shown in Fig. 12, the rise of heating temperature leads to an increase of the temperature gradient (G_L) in the liquid of the mushy zone, so the primary and secondary dendrite arm spacings diminish at different positions on the same cross section of the specimen (Fig. 6 and Fig. 8(a)).

It should be noted that when deriving Eqs. (2) and (3), the solidification interface was considered to be horizontal, so G_L goes down to the opposite direction of solidification. MILLER and POLLOCK [28] found that lateral heat dissipation could change the morphology of dendrites, leading to lateral growth of dendrites. This means that the morphology of dendrites is not only affected by the above-mentioned temperature gradient in the vertical direction and solidification rate, but also affected by lateral heat dissipation. As shown in Fig. 13, in this research, the sloping isotherm from the outer side to the inner implies the existence of large lateral heat extraction of the outer side and the lateral temperature gradient component G_x (Fig. 10), which may be the reason why the secondary dendritic arm near the outer side is longer and slimmer than that near the inner side and the center of cross section (Fig. 7). The existence of lateral

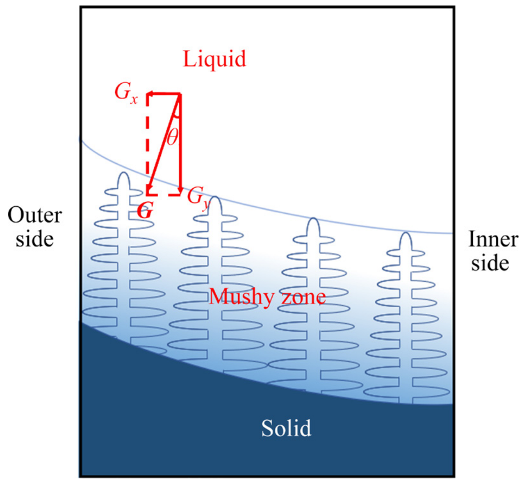

Fig. 13 Morphology of mushy zone on right side of first stair

temperature gradient component (G_x) reduces the vertical temperature gradient component G_y=$G\cos\theta$, which leads to the diminish of PDAS. The mushy zone exhibits a concave and sloping state (Fig. 10), so the inclination angle (θ) of the isotherm is larger and the vertical temperature gradient component (G_y) is smaller as it is closer to the two sides. This is the reason why the PDAS in the same cross-section near the outer side is larger than that near the inner side and the center part (Fig. 8(a)).

The formation of the eutectics in the single crystal superalloys is related to the segregation of Al and Ta [29]. As solidification progresses, Al and Ta are expelled into the inter-dendritic region. When the composition reaches the eutectic composition and the temperature reaches the eutectic precipitation temperature, the eutectics will precipitate. The formation of eutectics depends on the degree of element segregation. The segregated degree of Al and Ta is determined by the diffusion time ($\Delta T/(GR)$) and the diffusion distance ($\lambda_1/2$). With the increase of the heating temperature, the cooling rate (GR) of the liquid in the mushy zone increases. This will shorten the diffusion time of the element in the inter-dendritic region and increase the tendency of element segregation. On the contrary, the PDAS (λ_1) decreases with the growth of the heating temperature (Fig. 8(a)). This will shorten the diffusion distance ($\lambda_1/2$) of the element and promote the homogenization of the elements. Affected by these two opposite factors, the volume fraction of eutectics changes little when the heating temperature is increased to 1570 °C (Fig. 8(b)).

The cooling rate in the outer side of the specimen is larger than that of the inner side when the solidification progresses to the first stair (Fig. 10) and the PDAS (λ_1) near the outer side is also larger than that near the inner side, so the diffusion time ($\Delta T/(GR)$) of the elements will be shortened and the diffusion distance ($\lambda_1/2$) will be larger near the outer side of the specimen. This is the reason why the volume fraction of the eutectics near the outer side is significantly higher than that near the inner side (Fig. 8(b)).

4.3 Effects of shell mold heating temperature on formation of freckles

As shown in Fig. 3, no any freckle appears on the second and third stairs of the specimen at the two shell mold heating temperatures, and freckles are only formed on the first stair. This is influenced by casting size and morphology of isotherm in the freckle formation. The increase of casting size and the inclination angle of isotherm promotes the tendency of freckle formation [24]. Freckles are not formed in the second stair of specimen when the shell mold heating temperature is 1510 °C, but are formed in the first stair of specimen when the shell mold heating temperature gets to 1570 °C (Fig. 3(a)), although the two stairs have almost similar mushy zone height (Table 4) and solidification parameters (Table 6 and Table 7) during solidification. This is caused by the different inclination angles of the isotherm in the mushy zone. The average inclination angle of the isotherm is 4.3°±0.3° in the second stair of specimens at 1510 °C while it is 7.6°±0.6° in the first stair of specimen at 1570 °C (Table 5 and Fig. 11(b)). The inclination angle of the isotherm has nearly doubled, which will increase the tendency of the freckle formation.

A large number of studies have shown that freckles are caused by dendrite fragmentation or remelting due to the thermal-solutal convection in the mush zone [30,31]. In this research, a large amount of dendritic fragments with disordered orientation can be observed in the freckled area (Fig. 5), so it is reasonable to speculate that thermal-solutal convection has occurred in the mushy zone during the solidification of the specimen in the two different heating temperature conditions. The resistance to the flow of the melt in the mushy zone can be expressed by the permeability (K), which can be calculated by the following Eqs. (4) and (5) [32]:

$$K_y = 3.75\times10^{-4} f_L^2\lambda_1^2 \quad (0.17<f_L<0.61) \tag{4}$$

$$K_x = 3.62\times10^{3} f_L^{3.34}\lambda_1^{0.669}\lambda_2^{2.73} \quad (0.19<f_L<0.66) \tag{5}$$

where K_y is the permeability of the liquid along the primary dendritic arm, while K_x is the permeability of the liquid along the secondary dendritic arms. The larger the permeability K is, the lower the resistance of the dendrites structure is to the liquid flow. From Eqs. (4) and (5), it can be deduced that the resistance of the dendrites to the liquid flow rises with the decrease of the PDAS (λ_1) and SDAS (λ_2). PDAS (λ_1) and SDAS (λ_2) both diminish with the increase of the heating temperature (Figs. 6 and 8(a)), so the permeability of the melt in the mushy zone decreases, which weakens the strength of liquid convection and reduces the tendency of freckle formation.

The decrease of dendrite arm spacing increases the resistance of liquid convection, and narrows the liquid convection channel. The width of the convection channel determines the width of the freckle chains, so the width of the freckle chains is reduced significantly when the shell mold heating temperature increases from 1510 to 1570 °C (Fig. 5). The strength of the liquid convection determines the number of dendrite fragments in the mushy zone, so less dendritic fragments are found in the freckled area at the heating temperature of 1570 °C. In addition, as the shell mold heating temperature rises, the cooling rate of the liquid in the mushy zone increases, which will shorten the local solidification time of the melt in the mushy zone and weaken the tendency of the fragmentation or remelting of the dendrites by the liquid flow in the mushy zone. This will further reduce the number of dendrite fragments in the freckled area.

5 Conclusions

(1) With the increase of shell mold heating temperature, the propensity of freckle formation is reduced, and the width of freckle chains and number of dendritic fragments in freckled region significantly decrease.

(2) The reduced dendritic arm spacings lower the permeability of the liquid in the mushy zone at higher shell mold heating temperature and impair the strength of the liquid convection in the mushy zone, resulting in a lower tendency to freckle formation.

(3) The increase of the shell mold heating temperature reduces the height of the mushy zone especially for the first stair with larger size and causes a shortened local cooling time of the liquid in the mushy zone, which further weakens the fragmentation or remelting of dendrite by the liquid flow.

CRediT authorship contribution statement

Zhi-cheng WANG: Performing experiments, Investigation, Methodology, Formal analysis, Writing − Original draft, Review & editing; **Jia-rong LI:** Conceptualization, Supervision, Project administration, Funding acquisition, Review & editing; **Shi-zhong LIU:** Resources, Review & editing, Validation; **Wan-peng**

YANG: Review & Editing; **Xiao-guang WANG:** Review & editing.

Declaration of competing interest

The authors declare that they have no known competing financial interests or personal relationships that could have appeared to influence the work reported in this paper.

Acknowledgments

This work was supported by the National Science and Technology Major Project of China (Nos. 2017-VI-0001-0070, J2019-III-0008-0052).

References

[1] CETEL A D, DUHL D N. Second-generation nickel-base single crystal superalloy [C]// Proc Superalloys 1988. Warrendale, PA: TMS, 1998: 235−244.

[2] HARRIS K, ERICKSON G L, SIKKENGA S L, BRENTNALL W D, AURRECOECHEA J M, KUBARYCH K G. Development of the rhenium containing superalloys CMSX-4 and CM186LC for single crystal blade and directionally solidified vane applications in advanced turbine engines [C]// Proc Superalloys 1992. Warrendale, PA: TMS, 1992: 297−306.

[3] WALSTON W S, OHARA K S, ROSS E W, POLLOCK T M, MURPHY W H. RenéN6: Third generation single crystal superalloy [C]// Proc Superalloys 1996. Warrendale, PA: TMS, 1996: 27−34.

[4] LI Jia-rong, LIU Shi-zhong, WANG Xiao-guang, SHI Zhen-xue, ZHAO Jin-qian. Development of a low-cost third generation single crystal superalloy DD9 [C]// Proc Superalloys 2016. Warrendale, PA: TMS, 2016: 57−63.

[5] ZHANG Jun, HUANG Tai-wen, LIU Lin, FU Heng-zhi. Advances in solidification characteristicsand typical specimen defects in nickel-based single crystal superalloys [J]. Acta Metallurgica Sinica, 2015, 51(10): 1163−1178.

[6] ZHOU Yi-zhou, GREEN N R. Competitive grain growth in directional solidification of a nickel-base superalloy [C]// Proc Superalloys 2008. Warrendale, PA: TMS, 2008: 317−324.

[7] HAN Dong-yu, Jiang Wei-guo, XIAO Jiu-han, LI Kai-wen, LU Yu-zhang, LOU Lang-hong. Investigating the evolution of freckles into sliver defects in Ni-based single-crystal superalloy castings [J]. Materials Today Communications, 2021, 27: 1−14.

[8] WANG Zhi-cheng, LI Jia-rong, LIU Shi-zhong, Zhao Jin-qian, SHI Zhen-xue, WANG Xiao-guang, YANG Wan-peng, YUE Xiao-dai. Research progress in freckles of single crystal superalloys [J]. Journal of Materials Engineering, 2021, 49(7): 1−9.

[9] YANG Wan-peng, LI Jia-rong, LIU Shi-zhong, SHI Zhen-xue, Zhao Jin-qian, WANG Xiao-guang. Orientation dependence of transverse tensile properties of nickel-based third generation single crystal superalloy DD9 from 760 °C to 1100 °C [J]. Transactions of Nonferrous Metals Society of China, 2019, 29: 558−568.

[10] REED R C, TAO T, WARNKEN N. Alloys-By-Design: Application to nickel-based single crystal superalloys [J]. Acta Materialia, 2009, 57(19): 5898−5913.

[11] AUBURTIN P, COCKCROFT S L, MITCHEL A, WANG T. Freckle Formation in Superalloys [C]// Proc Superalloys 2000. Warrendale, PA: TMS, 2000: 255−261.

[12] AUBURTIN P, WANG T, COCKCROFT S L, MITCHELL A. Freckle formation and freckle criterion in superalloy specimens [J]. Metallurgical and Materials Transactions B, 2000, 31: 801−811.

[13] SAAD A, GANDIN C A, BELLET M, SHEVCHENKO N, ECKERT S. Simulation of channel segregation during directional solidification of In−75wt.%Ga qualitative comparison with in situ observations [J]. Metallurgical and Materials Transactions A, 2015, 46: 4886−4897.

[14] CHMIELA B, SOZANSKA M, CWAJNA J. Identification and evaluation of freckles in directionally solidified specimen made of PWA1426 nickel-based superalloy [J]. Archives of Metallurgy and Materials, 2012, 57(2): 559−564.

[15] POLLOCK T M, MURPHY W H, GOLDMAN E H, URAM D L, TU J S. Grain defect formation during directional solidification of nickel base single crystals superalloys [C]// Proc Superalloys 1992. Warrendale, PA: TMS, 1992: 125−134.

[16] POLLOCK T M, MURPHY W H. The breakdown of single-crystal solidification in high refractory nickel-base alloys [J]. Metallurgical and Materials Transactions A, 1996, 27: 1081−1094.

[17] MA De-xin, POLACZEK A B. The geometrical effect on freckle formation in the directionally solidified superalloy CMSX-4 [J]. Metallurgical and Materials Transactions A, 2014, 45: 1435−1444.

[18] HONG Jian-ping, MA De-xin. WANG Jun, WANG Fu, DONG An-ping, SUN Bao-de, POLACZEK A B. Geometrical effect of freckle formation on directionally solidified superalloy CM247 LC components [J]. Journal of Alloys and Compounds, 2015, 648: 1076−1082.

[19] MA De-xin, ZHOU Bin, POLACZEK A B. Investigation of freckle formation under various solidification conditions [J]. Advanced Material Research, 2011, 278: 428−433.

[20] HAN Dong-yu, JIANG Wei-guo, XIAO Jiu-han, LI Kai-wen, LU Yu-zhang, ZHENG Wei, ZHANG Shao-hua, LOU Lang-hong. Investigation on freckle formation and evolution of single-crystal nickel-based superalloy specimens with different thicknesses and abrupt cross-section changes [J]. Journal of Alloys and Compounds, 2019, 805: 218−228.

[21] MA De-xin, MATHES M, ZHOU Bin, POLACZEK A B. Influence of crystal orientation on the freckle formation in directionally solidified superalloys [J]. Advanced Material Research, 2011, 278: 114−119.

[22] SZELIGA D. Effect of processing parameters and shape of blade on the solidification of single-crystal CMSX-4 Ni-based superalloy [J]. Metallurgical and Materials Transactions B, 2018, 49: 2550−2570.

[23] MILLER J D, POLLOCK T M. The effect of processing conditions on heat transfer during directional solidification via the Bridgman and liquid metal cooling processes [J].

Metallurgical and Materials Transactions A, 2014, 45: 411−425.

[24] WANG Zhi-cheng, LI Jia-rong, LIU Shi-zhong, ZHAO Jin-qian, WANG Xiao-guang, YANG Wan-peng. Investigation on freckle formation of nickel-based single crystal superalloy specimens with suddenly reduced cross section [J]. Journal of Alloys and Compounds, 2022 918: 165631.

[25] LI Jia-rong, LIU Shi-zhong, SHI Zhen-xue, LUO Yu-shi, WANG Xiao-guang. Third generation single crystal superalloy DD9 [J]. Journal of Iron and Steel Research, 2011, 23(2): 337−340.

[26] KURZ W, FISHER D J. Fundamentals of Solidification [M]. 4st ed. Enfield: Trans Tech Publications, 1998.

[27] HUNT J D. Solidification and Specimen of Metals [M]. London: The Metalsa Society, 1979.

[28] MILLER J D, POLLOCK T M. Stability of dendrite growth during directional solidification in the presence of a non-axial thermal field [J]. Acta Materialia, 2014, 78: 23−36.

[29] HECKL A, RETTIG R, CENANOVIC S, GOKEN M, SINGER R F. Investigation of the final stages of solidification and eutectic phase formation in Re and Ru containing nickel-base superalloys [J]. Journal of Crystal Growth, 2010, 312: 2137−2144.

[30] YUAN L, LEE P D. A new mechanism for freckle initiation based on microstructural level simulation [J]. Acta Materialia, 2012, 60: 4917−4926.

[31] REN Neng, PANWISAWAS C, LI Jun, XIA Ming-xu, DONG Hong-biao, LI Jian-guo. Solute enrichment induced dendritic fragmentation in directional solidification of nickel-based superalloys [J]. Acta Materialia, 2021, 215: 117043.

[32] PHILIPPE B. Determination of the influence of growth front angle on freckle formation in superalloys [D]. Vancouver: University of British Columbia, 1998: 16−22.

型壳加热温度对单晶高温合金显微组织及“雀斑”形成的影响

王志成，李嘉荣，刘世忠，杨万鹏，王效光

北京航空材料研究院 先进高温结构材料重点实验室，北京 100095

摘　要：利用所设计的阶梯试样进行定向凝固试验和模拟，研究定向凝固过程型壳加热温度对单晶高温合金铸件显微组织和“雀斑”形成的影响。分析糊状区的温度场及形貌。结果表明，升高型壳加热温度，一次和二次枝晶间距减小，糊状区液相的渗透率和对流通道的宽度降低，“雀斑”形成倾向性降低，“雀斑”宽度减小，“雀斑”区域枝晶碎片减少。此外，随着型壳加热温度的升高，糊状区液相冷却速率增加，糊状区熔体的冷却时间减少，液体流动对枝晶的破碎程度得到削弱，这进一步降低单晶高温合金铸件“雀斑”形成的倾向性。

关键词：单晶高温合金；“雀斑”形成；型壳加热温度；定向凝固；数值模拟

(Edited by Bing YANG)